FTIR Imaging Studies of a New Two-Step Process To Produce Polymer Dispersed Liquid Crystals

Rohit Bhargava, Shi-Qing Wang, and Jack L. Koenig*

Department of Macromolecular Science, Case Western Reserve University, Cleveland, Ohio 44106

Received September 30, 1998; Revised Manuscript Received December 22, 1998

ABSTRACT: Polymerization-induced phase separation (PIPS) to produce PDLCs is usually carried out in the one-phase regime to obtain the final dispersion. This PIPS process results in significant residual liquid crystal solubility in the matrix. We investigate a new method to reduce liquid crystal solubility by cooling a homogeneous liquid crystal/precursor mixture into the two-phase regime followed by fast matrix polymerization. The proposed procedure is tested by using a well-studied PDLC system—NOA65 and E7. Liquid crystal remaining dissolved in the matrix is sharply reduced by this method. Residual solubility of the matrix material in liquid crystal domains is also decreased. While maintaining the same phase composition, the method also allows tailoring dispersion size according to needs as opposed to the invariable correlation between droplet size, solubility, and polymerization rate inherent in the classical PIPS methods. This general methodology could be usefully applied to other systems. FTIR imaging, combined with statistical methods, is shown to be an extremely valuable tool for determining phase composition in multiphase systems.

Introduction

Polymer dispersed liquid crystals (PDLCs) are composed of low molecular weight liquid crystal (LC) microdomains in a polymeric matrix. Devices incorporating PDLCs have a wide variety of applications in the electrooptical industry[1] and as light modulators in windows and displays, mainly due to potential difference modulated, reversible light scattering by dispersed liquid crystal domains. As opposed to twisted and supertwisted nematic devices, they do not require alignment layers, stringent thickness control, or polarizers. This results in brighter and more compact equivalent systems, which are fabricated with greater ease.

PDLC films are prepared by inducing phase separation in an initially homogeneous mixture of a liquid crystal and a polymer or polymer precursor. The phase separation phenomenon is the single most important step for efficient fabrication of PDLC devices from a given set of materials. Phase separation may be brought about by polymerization-, thermal-, or solvent-induced methods.[2] Solvent evaporation-induced phase separation (SIPS) involves handling and disposal of solvents during a process. This is not preferred from a safety and environmental point of view. Moreover, convection effects during evaporation of the solvent may cause spatial ordering and a preferred orientation of liquid crystal droplets.[3] Thermally induced phase separation (TIPS) involves the need for good temperature control and stabilization. Morphology of systems containing a low-T_g matrix may change with temperature.[4] In such cases, LC domains undergo Ostwald ripening and coalescence, which requires surface-active agents to stabilize the dispersed phase.[5] These surface-active agents lower interfacial tension and, consequently, would result in a higher solubility of LC in the thermoplastic matrix. High-T_g matrices will contain high residual solubility due to phase separation induced at higher temperatures where matrix chain mobility is higher. The number of polymers suitable for the TIPS technique is limited by their (high) solubility with the liquid crystal for the operating temperature range. Polymerization-induced phase separation (PIPS) does not involve use of solvents and usually maintains attained morphology due to extensive cross-linking in the matrix. Among the various methods of inducing phase separation, PIPS appears to be the most attractive route to prepare PDLCs. Thermally curable systems are expected to have a high liquid crystal solubility in the matrix due to curing at high temperatures. Photoinduced polymerization of the matrix is a preferred route as it allows independent control over the temperature and the cure rate. UV curable oligomeric mixtures have been used to prepare PDLCs due to the high degree of control achieved by the UV process.[6] The polymerization process, solubility, and size of the dispersed phase are inseparably linked in such systems. All the above methods result is significant solubility of the liquid crystal in the matrix. Liquid crystal solubility in the matrix has been estimated to be high with typical values being of the order of 30−50%, e.g., over 40% for 7CB in PMMA and over 30% in PS,[7] 25%−30% for E7 in PBMA,[12] and about 30% for E7 in NOA65 at room temperature.[8]

While a liquid crystal−monomer solution may be used as a starting material in photoinduced PIPS, an oligomer−liquid crystal mixture is preferred due to low oligomer volatility and no loss in handling ease. When this mixture is cured, a significant fraction of the mixed liquid crystal remains dissolved in the matrix, leading to plasticization of the matrix and waste of the liquid crystal. Some matrix material may also remain trapped in the liquid crystal droplets,[9] lowering the nematic−isotropic temperature, possibly causing defects and degrading performance properties. More importantly, this mutual solubility may also change the carefully matched refractive indices of the phases[10,11] leading to poor device performance and deviation from intended properties. Thus, a methodology to reduce mutual solubilities of the two phases is not only of commercial importance but is also an interesting fundamental issue with applications for polymeric multicomponent phase separated systems.

10.1021/ma981542s CCC: $18.00
Published on Web 03/20/1999

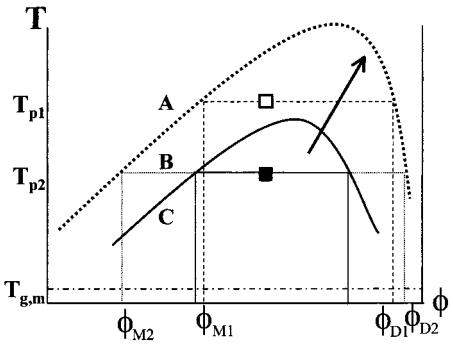

Figure 1. Generic phase diagram showing the coexistence curve and solubility for uncured oligomer−LC (solid line) and curing PDLC (dashed line).

Studies examining the issue of solubility of liquid crystal in the matrix have been carried out both experimentally[12] and theoretically.[13−15] Efforts to reduce miscibility typically center on the search for new LC−polymer systems that have reduced mutual solubility. Neglecting the two-phase regime, it has been implied that selecting a suitable LC−polymer combination that forms an initially homogeneous phase at the temperature of formation can lower solubility.[16] Using this approach, extensive analyses have been carried out to determine optimum properties for such combinations.[17,18] Thus, a process with a general methodology that can use any given set of materials to achieve reduced LC solubility with minor process adjustments will be attractive.

Most oligomer−LC systems of interest for PDLC formation exhibit an upper critical solution temperature (UCST) type of phase behavior.[13,14] PDLCs are prepared above the cloud point of the starting materials. For a PDLC system formed by using an ultraviolet curable precursor, the matrix cure rate depends on UV intensity with the cure temperature playing a minor role in the polymerization process. However, given a particular cure state of the matrix, temperature is a major process variable in the phase separation process. In this paper, we will investigate the effect of temperature on the phase separation process for PDLC formation involving polymerization.

The Proposed Method. A typical UCST curve for a curing oligomer−liquid crystal mixture is shown in Figure 1. The solid lines represent the state prior to curing, and the dashed lines represent the postcuring state. The coexistence curve in such phase diagrams defines one-phase and two-phase regions. Upon polymerization, the coexistence curve shifts toward higher temperatures in the direction of the arrow to the curve close to matrix gelation shown as a dashed curve. Clearly, there are different regions of interest in temperature−composition space that may influence formation and the ultimate properties of the PDLC. A mixture in region A will not phase separate even after extensive polymerization. Starting from a homogeneous mixture in region B (between the coexistence curves), one obtains a phase-separated PDLC system after polymerization due to the coexistence curve now being the dashed one for the polymerized matrix−liquid crystal system. The very appearance of two phase-separated dispersions implies that the time scale for phase separation is faster than that for polymerization to gelation. However, it is not clear whether the time scale for phase separation is fast enough for residual solubility to be determined only by thermodynamic equilibrium conditions. It has been proposed that phase separation in this process is fast and may occur at much lower conversion, i.e., well before gelation.[19] In the case of fast polymerizing systems, which reduces the process time, significant solubility may be present due to kinetic factors. It is in region B that all PDLCs currently are made via PIPS.[20] Ever since the first PDLC formed by this methodology,[21] a homogeneous solution is emphasized as the first goal[2,20,22] and a phase-separated structure the result of the formation process. It is speculated that if the initial mixture is in region C, it will phase separate before polymerization and may have undesirable structures.[23]

A liquid crystal−oligomer mixture in region C will phase separate even before polymerization. However, they will not instantaneously separate into two domains of liquid crystal and oligomer. The extent of phase separation and the size of such phase-separated domains would depend on the kinetics of phase separation. Thus, it has not been obvious whether polymerizing in this region is indeed undesirable. The composition of the phase-separated domains at any temperature can be given by tie lines to the coexistence curve at that temperature (see Figure 1). For polymerizing at temperature T_{p1} and a lower temperature, T_{p2}, compositions of the two formed phases can be seen. A large difference results in compositions of the two phases formed after curing simply by lowering the temperature. Significantly lower amounts of liquid crystal will remain dissolved in the matrix after polymerization at the lower temperature and subsequent use at higher temperatures. Residual solubility of matrix material is also expected to be lower. On the basis of these observations, a new route to produce PDLCs resulting in lower matrix solubilities may be suggested.

The new process, termed TICS (thermally induced curing stabilization) phase separation, would involve cooling the unpolymerized matrix−LC mixture to the two-phase region (e.g., to temperature T_2 in Figure 1), allow sufficient time for phase separation, and subsequently polymerize the dispersion rapidly at the lowered temperature. The polymerization would "freeze in" the formed structures, thereby maintaining solubility at levels below that obtained from carrying out the process at higher temperatures. A well-studied system[24,25,33] (photocurable, thermosetting matrix, NOA65 and liquid crystal, E7) which has high liquid crystal solubility is chosen as a model system to examine the route for PDLC formation by TICS phase separation. We fabricated PDLC films as described in the Experimental Section and examined resultant dispersions and residual LC solubility using FTIR imaging.

FTIR Imaging. FTIR microspectroscopy presents the most direct route to characterize spatial chemical variations in a sample and has been applied to PDLCs.[26,27] By monitoring the characteristic bands of a chemical species, its spatial distribution can be seen by means of a chemical image. Conventional infrared microspectroscopy uses apertures to limit the examined area and sequentially maps out the total spatial area. This technique not only is comparatively time-consuming but also lacks the spatial resolution obtained by infrared imaging using a focal plane array detector. FTIR imaging using a focal plane array detector has been recently introduced[28] and successfully used to obtain chemical images of PDLCs.[29] We used a focal plane array equipped spectrometer to study spatial distribution of

liquid crystal in PDLCs. This instrumentation is a powerful tool for examining dispersions of size greater than ~5 μm. FTIR imaging, having in-situ, noninvasive and nondestructive examination capabilities, appears to be an excellent method to examine solubility, being constrained only by the incident radiation wavelength-limited resolution.

Experimental Section

Infrared images were obtained using the Bio-Rad Stingray imaging spectrometer. It consists of the FTS 6000 step scan interferometer bench which is coupled to a focal plane array equipped microscope, UMA-500.[30] The imaging detector is a Santa Barbara focal plane mercury cadmium telluride (MCT) array of 64 × 64 elements imaging an average spatial area of 500 μm × 500 μm in a single experiment. To improve signal-to-noise characteristics, the instrument is equipped with a Germanium long pass filter to eliminate Fourier fold-over perturbations. A KRS-5 plate, which acts as a diffuser, is placed in the beam path before the condenser to further improve spatial homogeneity. Spectral and image processing is carried out by using a hyperspectral imaging software package, Environment for Visualizing Images (ENVI).[31] A spectral resolution of 4 cm^{-1} was used for the study. To improve signal-to-noise ratio, a number of image sets were co-added using ENVI. The number of frames averaged during spectrometer acquisition and images co-added during processing using ENVI were adjusted to obtain an error in the minimum measured relevant band intensity of no more than 3%.

Materials. The low molecular weight liquid crystal used in this study is E7,[32] a eutectic mixture of cyanobiphenyls. The mixture contains 51% *n*-pentylcyanobiphenyl (5CB), 25% *n*-heptylcyanobiphenyl (7CB), 16% *n*-octyloxycyanobiphenyl (8OCB), and 8% *n*-penyltcyanoterphenyl. The nematic−isotropic transition temperature of this system is reported to be about 333 K (60 °C), a smectic to nematic transition about 243 K (−30 °C), and a glass transition temperature of about 213 K (−60 °C). Being a multicomponent system, it does not freeze and usually forms a glass below the T_g. The polymeric matrix used in this study is a Norland UV-curable optical adhesive, NOA65.[33] NOA65 is reported to be a mixture composed primarily of trimethylolpropane diallyl ether, trimethylolpropane tris thiol, isophorone diisocyanate ester, and a benzophenone photoinitiator.[34] All materials were used as received. Mixtures by weight of LC and NOA65 were used to prepare the samples. The mixture was weighed, hand-mixed for 2 min, and heated to 85° C (well above the clearing point of E7) for 2 min and mixed again. Samples containing 10 μm diameter spacers were directly cast onto a NaCl salt plate and sandwiched by another salt plate. Glass coverslips were used as substrates for another set of samples. The sandwiched assembly was subjected to a constant weight for 15 min to apply pressure in order for it to attain hydrodynamic equilibrium. Constant spacing between the substrates was assured by sealing the sides with a two-part epoxy. Care was taken to see that there is no interaction between epoxy and the sample. After the epoxy had set, the samples were again heated above the clearing point for a minute and quenched to the desired temperature for the requisite period of time, after which it was subjected to UV radiation. UV radiation at a wavelength of 365 nm was obtained using a hand-held UV lamp. DSC scans were carried out to identify transitions E7, and temperatures of polymerization are chosen so as not to coincide with any transition in the liquid crystal.

Data and Data Analysis

To ensure that the sampling technique involving heating and cooling cycles did not degrade the components in any manner, infrared spectra of pure materials before and after heat treatments were analyzed. NOA-65 did not show any degradation even after heating for 5 min at 85° C. Cooling at 265 K for 24 h and dark storage light conditions did not affect the infrared spectrum of NOA-65 in any manner, and hence polymerization was carried out without further filtering out ambient light. Thus, any effects due to polymerization and/or degradation of the polymer or LC due to heating and cooling or exposure to light during preparation and storage for this study are ruled out.

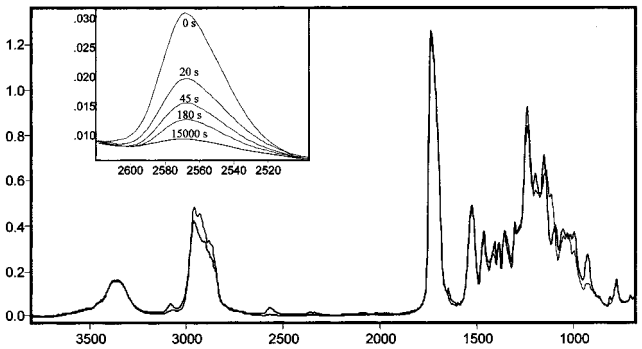

Figure 2. Spectra of cured (red line) and uncured (blue line) NOA65 and curing monitored as a function of time for the S−H stretching band absorbance decrease (inset).

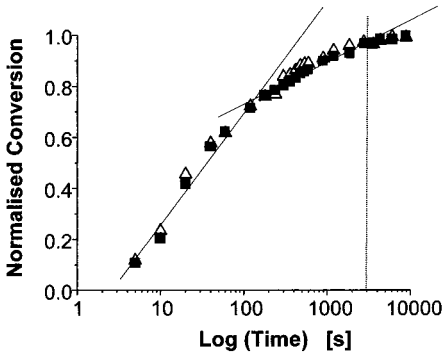

Figure 3. Neat NOA65 conversion based on S−H (■) stretching and C=C−H (△) stretching mode absorbance decrease.

The chemistry of the polymerization reaction for NOA65 is similar to that of a thiol−ene system.[35] Infrared absorption bands that correspond to the reacting species for such a reaction scheme can be readily identified and tracked in NOA65. The vinyl carbon stretching (~3070 cm^{-1}), sulfur−hydrogen stretching (~2570 cm^{-1}), or the carbon−carbon double-bond stretching (~1645 cm^{-1}) vibration may be monitored. Spectra of uncured NOA65 and of the sample cured for over 5 h at room temperature are shown in Figure 2. The inset shows the decrease in absorbance of the S−H stretching vibration at various UV exposure times. The vinyl carbon and hydrogen stretching candidates are also suitable for monitoring the reaction. Since the C=C stretching peak is weak and lies on the shoulder of a much stronger band, intensity changes are difficult to observe. Hence, suitable candidates to monitor the cure state are the other two bands. The conversion of the thiol and vinyl hydrogen stretching frequencies is plotted as a function of exposure to UV time in Figure 3. The kinetic information from the vinyl stretch and the thiol stretching vibration is in good agreement. Since the vinyl stretching band would not be very useful for the case of NOA65−liquid crystal mixtures, we will characterize the cure state of the matrix by examining the SH stretching band. From Figure 3, gelation can be seen to occur at a conversion of ~0.7 in about 2 min at room temperature. Conversion is over 90% of the final conversion in approximately 10 min.

The same cure state achieved in the same time interval serves as a basis for the study; i.e., the curing time scale is held constant for all temperatures. This approach would allow phase separation equilibrium to be attained quickly for higher temperatures from a kinetic point of view, as molecular mobility is higher. Thus, using the methodology outlined here, we are closer to the "worst case" scenarios for lower temperatures. Minor adjustments are made for curing UV intensity at different temperatures to get the same cure state of the matrix in the same time. This is readily achievable with a photocurable matrix of the NOA65 type. Liquid crystal−uncured NOA65 mixtures in the ratio 50:50 were cured at different temperatures. Preliminary tests were carried out to determine the UV intensity required to achieve a cure state greater than ∼80% in a curing time of 20 min.

Phase separation has been reported to occur for small polymerization times,[36] even when the cure is not complete. However, stable demixing is reportedly obtained at over 90% cure for the NOA65/E7 system.[37] The conversion of the thiol group in these experiments was of the order of 85%. Much longer times of cure would be needed to proceed to a greater conversion. Since it was the intention of the study to analyze the effect of prepolymerization time for a smaller curing time, this curing time and cure state achieved were considered satisfactory. No noticeable change was observed in these samples kept for over a month. In another set of samples prepared with about 40% conversion, domain coalescence (as evidenced by a decrease in number density of droplets and corresponding growth in average diameter), droplet growth, and increased sphericity of the droplets were noticed over a month long period. Hence, we assumed a cure state of over 85% to be of sufficient stability for the purpose of this study.

Infrared images of representative samples, obtained at different temperatures for increasing times of rest prior to polymerization, are seen in Figures 4 and 5. Figure 4 displays a set of images for samples cured after a prepolymerization rest time at 270 K for half to 8 h. Figure 5 displays the set for same time intervals at a rest temperature of 255 K. Careful attention must be paid to the manner in which IR images are plotted. In this paper, images are plotted as a ratio of the absorbance of a matrix specific band to the absorbance of the liquid crystal specific nitrile group stretching peak. Absorbance values are baseline and offset corrected. The ratio is then thresholded to give the maximum contrast between regions of the sample rich and poor in the species of interest. The limits used for color coding the images are shown on the two sets of images and have been mutually adjusted to give the same appearance. The limits are the same for all images in a set. From the limits, it is apparent that the composition of each phase is different in the two sets. The ratio representation used here not only normalizes the absorbance of a band relative to the other but also increases the thresholding limits making differences more prominent. Moreover, we have used glass spacer rods to control thickness of all samples studied. However, all experimental data and subsequent analysis are based on sample areas away from any spacer presence. This is done to exclude spacer effects on phase separation. It is conceivable that this would lead to an unequal thickness for various parts of a sample. Thickness variance may also be caused in areas close to air bubbles. Even in carefully controlled samples, a thickness deviation has been reported.[38] Some thickness variation is also seen in samples used in this study, and thus, the cell gap expected by use of spacers cannot be used as a constant for quantitative estimation with any great degree of certainty. Sample-to-sample variations of film thickness are seen to be small but cannot be ruled out a priori. To overcome this situation, band ratios of the two components, rather than absolute band absorbance values, are used to determine concentrations. These absorbance ratios, CR_M for the matrix and CR_D for the droplet, are also used to estimate the composition for each pixel in the image.

The band absorbance ratios introduced above are based on a band specific to each component that would maximize contrast between the phases. It is expected, and indeed found, that the solubility of liquid crystal in the matrix is more significant in the matrix than the matrix in the droplet. Here, the nitrile band (∼2227 cm^{-1}) is used as a basis for computation, and to maximize the difference in absorbance between the two phases while maintaining good signal-to-noise ratio even for small concentrations, the absorbance of the nitrile band was maximized by changing the sample thickness. A sample thickness of 10 μm was chosen as it was found to give a maximum absorbance of ∼0.7 au for the nitrile band. The matrix, NOA65, has a very strongly absorbing carbonyl stretching band at ∼1730 cm^{-1} and a broad weaker OH stretching band (∼3400 cm^{-1}). While maximizing absorbance in the linear region of the Beer−Lambert law for the nitrile band, it was noticed that in spatial regions of high NOA65 concentration, i.e., the matrix, the carbonyl stretching band was overabsorbing and nonlinear with concentration. For these concentrations, the OH stretching region displayed a sufficient absorbance for good signal-to-noise, and hence we use the relative absorbance of the OH stretching band and the nitrile band to estimate composition of the matrix. This ratio CR_M is then defined as

$$CR_M = A_{OH}/A_{CN} \tag{1}$$

where A_{CN} and A_{OH} are absorbance intensities characteristic to E7 and NOA65, respectively. For a given cell thickness, the absorbances for the nitrile and hydroxyl bands are expected to be linear with E7 concentration, w. They are written as functions of w,

$$A_{OH} = A^0_{OH} - m_2 w \tag{2}$$

$$A_{CN} = m_1 w \tag{3}$$

which implies that

$$CR_M^{-1} = \frac{m_1 w}{A^0_{OH} - m_2 w} \approx m_1 w (A^0_{OH} - m_2 w)^{-1} \approx m_1 w A^0_{OH} - m_1 m_2 w^2 \tag{4}$$

where the superscript "0" with absorbance indicates value at $w = 0$. Hence, to a first estimate, the fitting equation for CR_D and $(CR_M)^{-1}$ (with respect to LC weight fraction) for each concentration ratio is expected to be a quadratic passing through the origin. $(CR_M)^{-1}$ is plotted against w as the curve will then pass through the origin for neat NOA65. A similar analysis is carried out for the droplet regions. Absorbance of the OH stretching band was very small and in many cases is

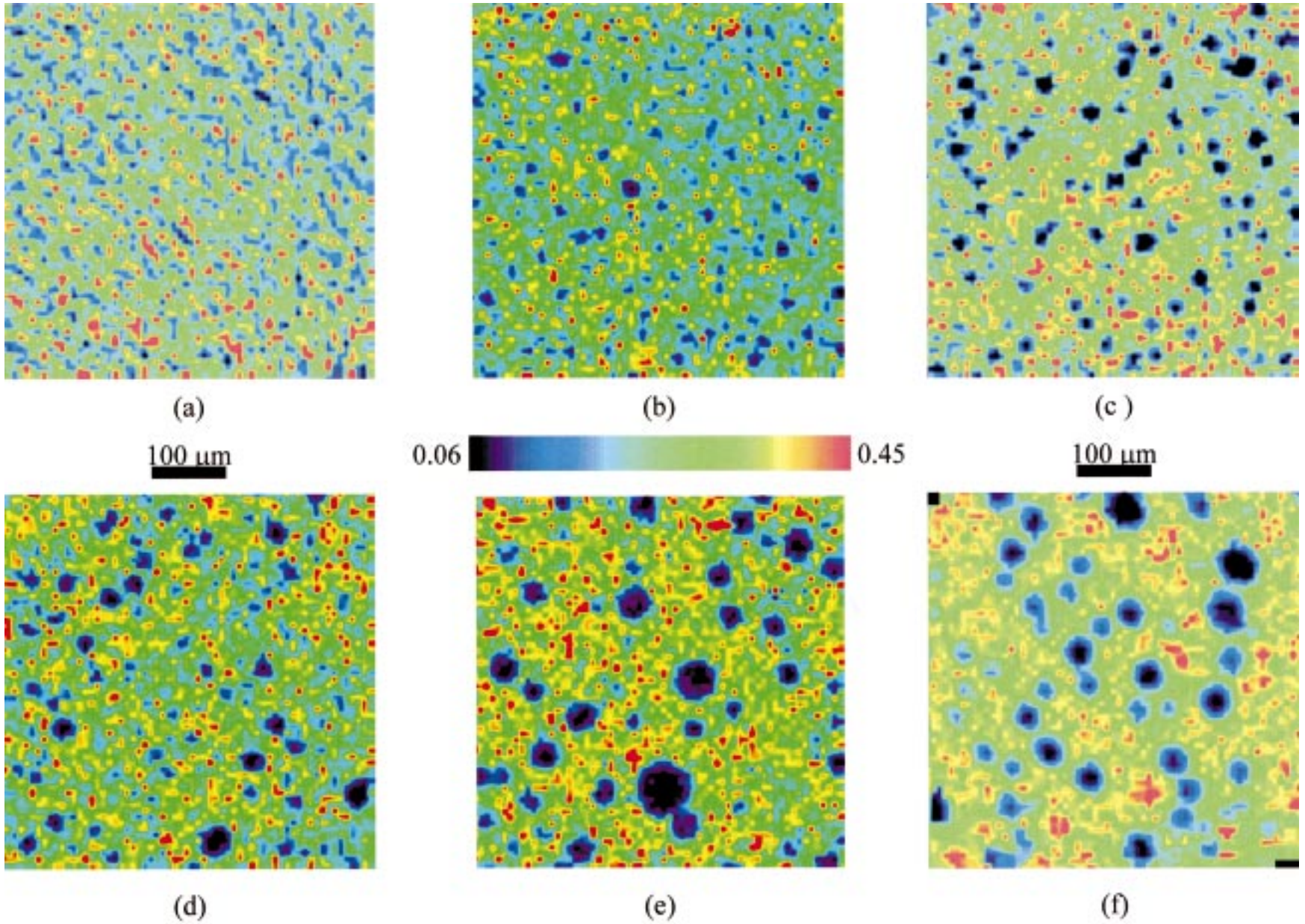

Figure 4. Infrared images of PDLCs formed by curing at 270 K after a prepolymerization cooling time of (a) 30 min, (b) 1 h, (c) 2 h, (d) 4 h, (e) 6 h, and (f) 8 h.

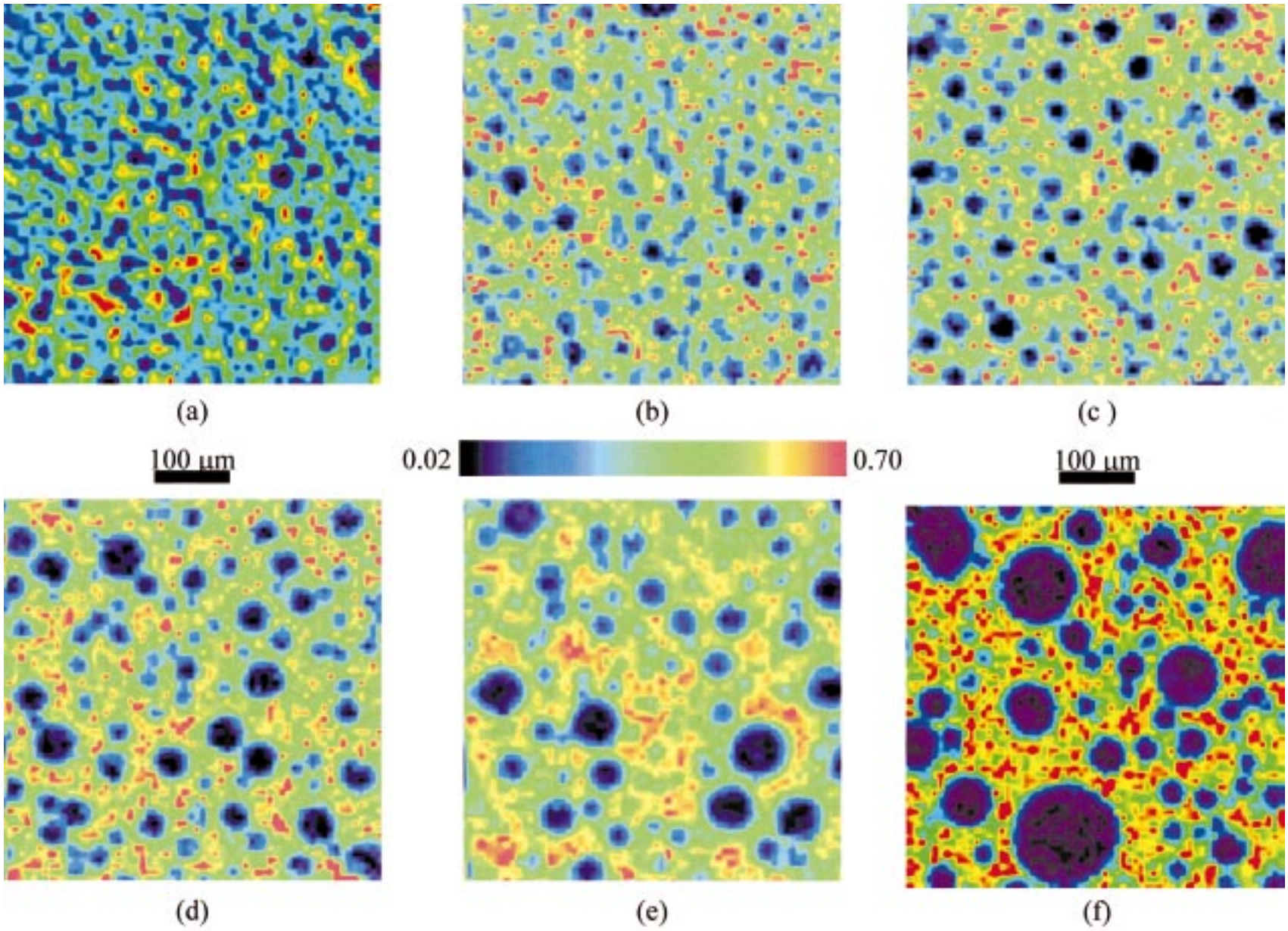

Figure 5. Infrared images of PDLCs formed by curing at 255 K after a prepolymerization cooling time of (a) 30 min, (b) 1 h, (c) 2 h, (d) 4 h, (e) 6 h, and (f) 8 h.

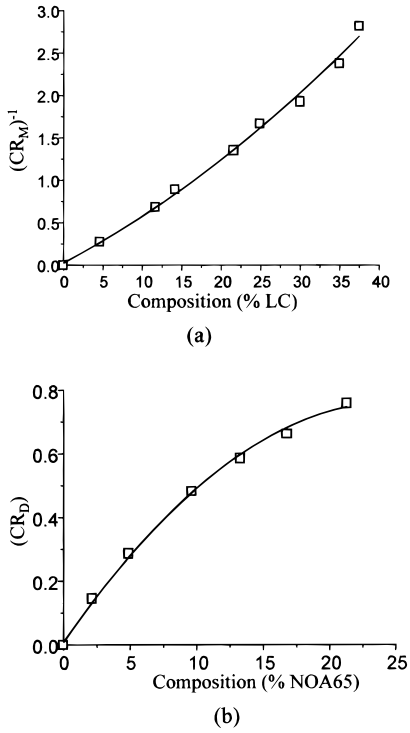

Figure 6. Calibration curve for (a) NOA65-rich phase (matrix) and (b) liquid crystal-rich phase (droplet) composition as a function of the minor component fraction.

smaller than the limits of detection (typically, 3 times the error). For LC droplets, the carbonyl region (characteristic only of NOA65) had an absorbance large enough for a good signal-to-noise ratio. Hence, the concentration ratio CR_D is defined as

$$CR_D = A_{CO}/A_{CN} \tag{5}$$

where A_{CO} is the absorbance intensity of the carbonyl peak.

Samples of known composition were prepared for various liquid crystal and matrix weight fractions and composition ratios obtained as a function of LC fraction or NOA65 fraction. These curves are shown in Figure 6a,b. The best quadratic equations of fit, the prediction equations for pixel composition, and goodness of fit are tabulated in Table 1. Fitting equations for the composition ratio as a function of weight fractions for the experimental points are given by

$$CR_M^{-1} = aw^2 + bw \tag{6a}$$

or

$$CR_D = aw^2 + bw \tag{6b}$$

and the prediction equation for composition, c (% LC or % NOA65), from the fitted curves is of the form

$$c\ (\%\ \mathrm{LC}) = i(CR_M^{-1})^2 + j(CR_M{}^{-1}) \tag{7a}$$

$$c\ (\%\ \mathrm{NOA65}) = iCR_D^2 + jCR \tag{7b}$$

The curves fitted to known composition are well predicted by a polynomial of degree 2 in LC fraction.

Table 1. Parameters and Goodness of Fit for Fitting and Inverse Prediction Equations

parameter	droplet	matrix
fitting equation		
a	−0.001	0.0005
b	0.0620	0.0515
R^2	0.998	0.994
prediction equation		
i	26.241	−1.613
j	8.049	18.140
R^2	0.997	0.994

Consequently, the prediction equation for composition, given a concentration ratio, is expected to be highly accurate.

The error in composition determination is due largely to error in absorbance ratios caused by instrumental noise in band absorbance. Noise in absorbance by a focal plane array may be broadly classified to be of three distinct types: spectral, spatial, and temporal. Spectral noise, or the uncertainty in absorbance, is estimated by the peak-to-peak noise in the baseline on either side of the absorption band. Since we are interested in the maximum magnitude of the error, the larger of the two noise values obtained from either side of a band is taken to be noise associated with the band. Typical error levels and associated distributions are shown for each band in Figure 7a,b. The magnitude of noise is found to be the similar for both bands in all cases. There does not seem to be any correlation between the noise associated with the two bands (Figure 7c). Spatial variation of the noise is important as it would allow correlating error in each pixel to the error in the average absorbance. Examining the noise plotted as an image for each set, we did not see a spatial pattern (e.g., see Figure 7d). As a consequence, the average error in absorbance may be estimated by an average of the noise in the image corresponding to the band. Average error estimation also allows for elimination of noisy pixels. Pixels with more than 3 times the average noise are excluded from statistical analysis. Since we are not examining real time images, the only concern is whether a temporal error is introduced into the images due to a larger acquisition time for collection of multiple images. Temporal error, due to a small intensity drift over time, has been found to be fairly small over the time period of data acquisition comparable to our acquisition time. Thus, temporal error may be considered negligible in this study.

Noise in the baseline is approximated as the error in absorbance for the band at that pixel and the fractional error (say for the nitrile band) for the absorbance is given by

$$\delta A_{CN} = \epsilon_{CN}/A_{CN} \tag{8}$$

where ϵ_{CN} is the associated baseline noise.

The fractional error in composition ratio may be determined (say for the droplet phase) from fractional errors in constituent bands by

$$\delta CR_D/CR_D = [(\delta A_{CN})^2 + (\delta A_{CO})^2]^{1/2} \tag{9}$$

Thus, the error in composition determination (as justified by the high R^2 fit for the prediction equations) is directly related to the error in composition prediction

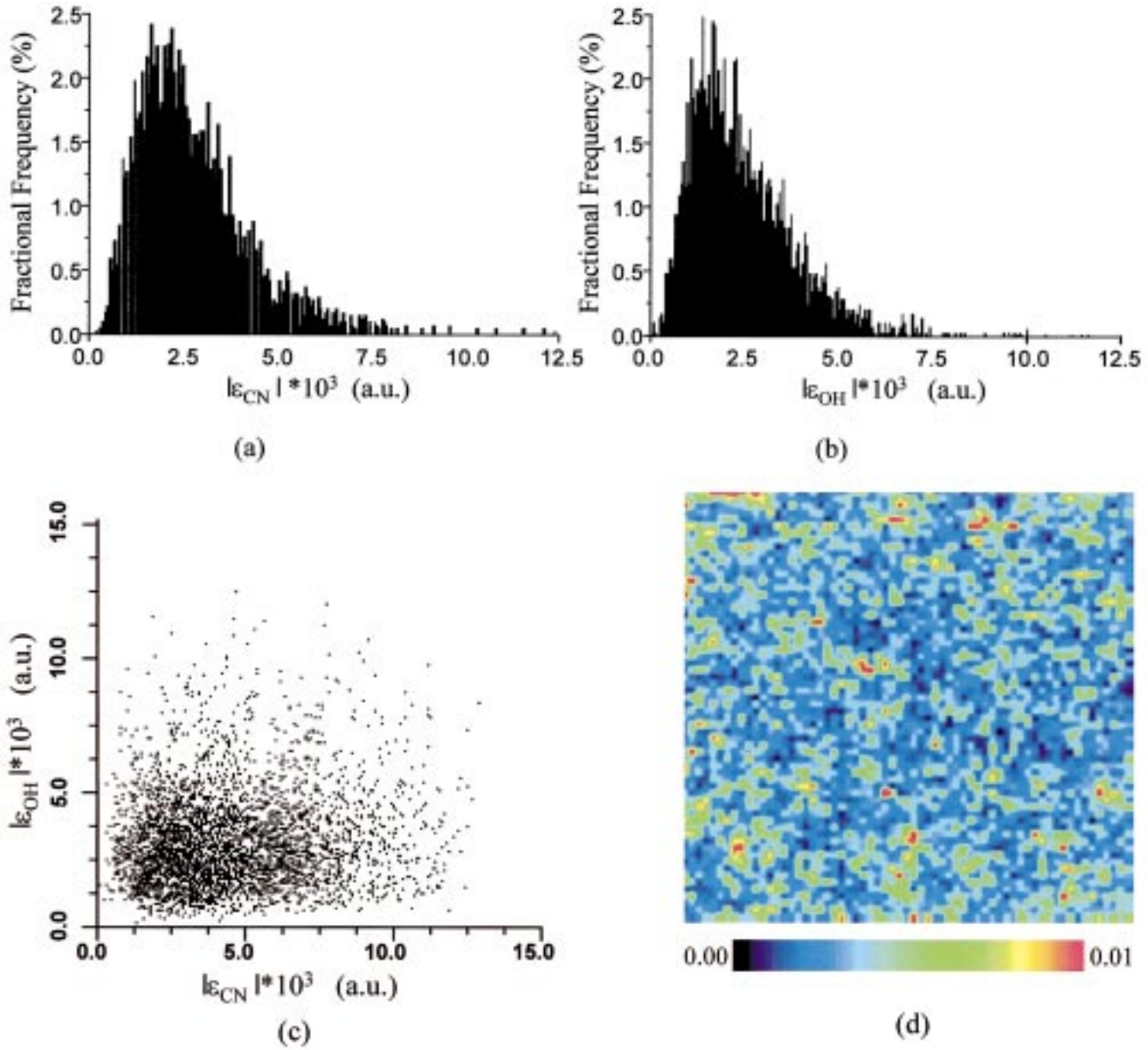

Figure 7. Modulus of noise associated with the (a) nitrile stretching band and (b) hydroxyl stretching band, (c) 2-D scatter plot of the modulus of noise of the hydroxyl band plotted versus the modulus of noise of the nitrile band, and (d) spatial distribution of noise intensities for the nitrile band.

for the matrix phase,

$$\delta c/\delta \mathrm{CR_M} = -3.226\mathrm{CR_M^{-1}} + 18.14 \qquad (10a)$$

And for the droplet phase,

$$\delta c/\delta \mathrm{CR_D} = 52.48\mathrm{CR_D} + 8.05 \qquad (10b)$$

These errors are used to extract composition ratios from the statistical data. Composition ratios themselves can be found by a variety of methods for each phase. Examining infrared images at different thresholds, an approximate number may be arrived at. For an estimate involving the error in measurement determined, one of the two methods suggested below may be followed. A histogram plot of the composition ratio may be constructed and the two peaks determined within 3 times the error for the composition ratio in that region. This would give the average phase composition within a 6σ limit. A typical histogram plot is shown in Figure 8a. This method is found to consistently allow at least 15% of all pixels into one of the two phases. Thus, as a rule of thumb, the two ratios may be deduced as the ones with at least 15% of the pixels higher (or lower in case of NOA65 solubility in E7) than the ratio value.

The method used plots the absorbance of a matrix specific band absorbance against the liquid crystal band absorbance. This 2-D plot shows two areas of high correlation point density as clusters at the extremes and a wide belt in the middle with relatively lower density (see for example Figure 8b). The two concentrations at the extremes represent the points due to the matrix and the droplets while the belt in the middle is due to the interphase. The two areas of high data point concentration are located with the help of an error ellipse. An ellipse is formed with its axis along the plot axis of a magnitude 6 times the error in measurement (approximated to the standard deviation) of the band plotted along the axis. This ellipse is then moved to

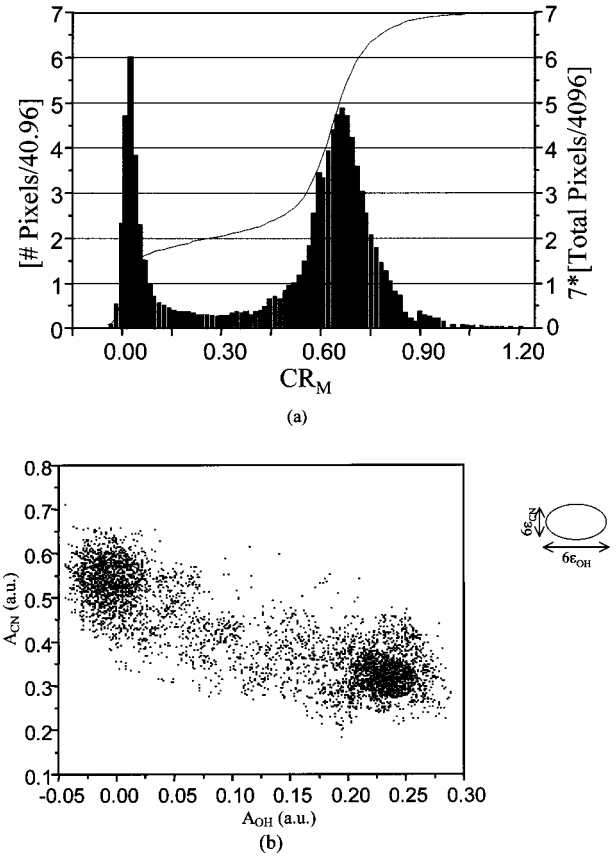

Figure 8. (a). Histogram showing the distribution of the composition ratio, CR_M, with the cumulative curve and error magnitude bar (b). 2-D scatter plot of the absorbance of the hydroxyl band versus the absorbance of the nitrile band. The error ellipse associated with the sample is shown on the side.

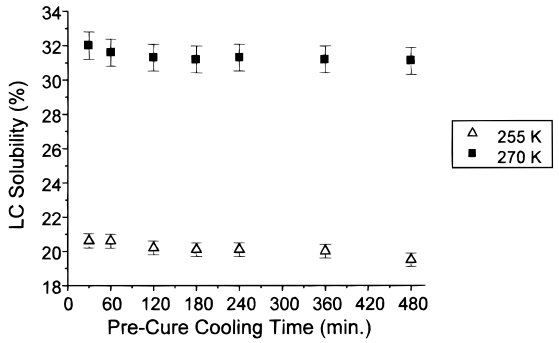

Figure 9. Matrix composition of PDLCs as a function of temperature.

cover the end lobes of the plot. The middle point of the ellipse is taken to be the average composition of the phase in question. Band ratios determined in this manner are converted to phase compositions using eqs 7a and 7b and plotted in Figures 9 and 10.

Results

Infrared images of representative samples, obtained at different temperatures for increasing times of rest prior to polymerization, are seen in Figures 4 and 5. Figure 4 displays a set of images for samples cured after a prepolymerization rest time at 270 K for $^1/_2$ to 8 h. Figure 5 displays the set for same time intervals at a rest temperature of 255 K. While similar topological features can be seen as in optical micrographs, additional information is provided about the chemical

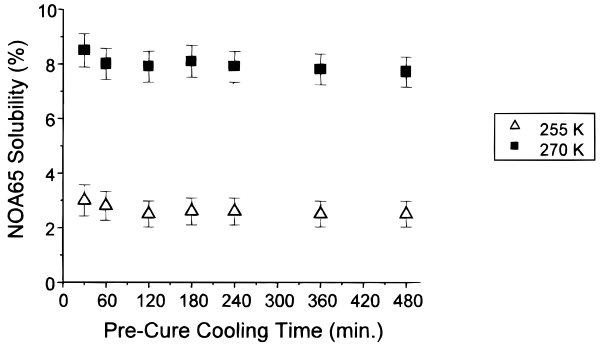

Figure 10. Droplet composition of PDLCs as a function of temperature.

distribution of the constituent materials. The average droplet diameter is seen to monotonically increase and the droplet density to decrease with rest time in both cases. This is possibly the result of increased coalescence. Droplet density and average droplet size are both greater for samples at 255 K. This points to reduced LC miscibility. Domain size distribution is also narrower for samples at 255 K. For larger cooling time samples' cured dispersions, we could not distinguish between spinodal decomposition followed by coalescence or diffusive transport and nucleation and growth. For smaller cooling times, a spatially regular pattern reminiscent of the early stage of spinodal decomposition concentration modulation may be discerned. Specifically, isoconcentration lines similar to those postulated in the case of spinodal decomposition[39] are seen. A morphological study of PDLCs prepared by the two-phase technique, including polarized microscopy studies, is reported elsewhere.[40]

The solubility of E7 in the NOA65 matrix is seen to decrease significantly by lowering the temperature (Figure 9). The error bars are obtained by using eqs 8−10 for each data point. There seems to be a small slope in both the curves. It is probably due to the imaged pixel size being larger than the droplet size and hence imaging both droplet and matrix areas. This is borne out as only the first data point, where droplet sizes are of the order of 10 μm, is significantly higher than the others in a temperature set. The same trend is also seen in Figure 10. This decrease in solubility is not significant enough to be concluded as a trend, and hence, it may be concluded that the matrix composition remains the same for all cooling times examined and depends only on the temperature. The solubility of NOA65 in E7-rich domains is seen to be rather small in both cases. Both high molecular weight for cured NOA65 and the nematic nature of liquid crystal droplets serve to lower the solubility of NOA65 in LC domains (Figure 1). In reducing solubility, gains are modest for the droplet phase as compared to that for the matrix phase due to the skewed nature of the polymer−LC coexistence curve. Solubility levels obtained by our methods are rather close to the approximated absolute limits of solubility reported for the E7/NOA65 precursor system. Solubility of E7 in the matrix is reported to be at least 15%, while that for NOA65 in E7 is reported to be about 5%.[41] While a polymerized matrix is indeed expected to have a lower solubility of the LC, a finite time required for phase separation (limited by gelation) as well as lower liquid crystal and matrix chain mobility at low temperatures may be expected to provide a counteracting effect. Thus, solubilities of about 20% appear to be

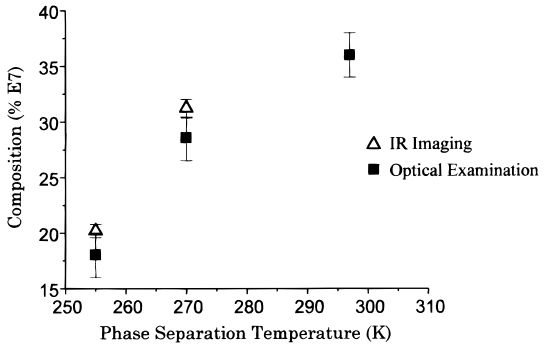

Figure 11. Comparison of solubility limits determined by infrared imaging and visual examination methods.

close to the limits achievable by any method. We may decrease temperature further to just above the glass transition of the liquid crystal (∼220 K) or matrix (∼210 K), but it is doubtful whether significant gains may be achieved by the lowering. A second set of data were obtained using glass coverslips as substrates, and data for matrix solubility of LC were found to match results using salt plates. Observation of the carbonyl group, and hence droplet composition determination, was not possible with the glass substrates.

Discussion

PDLC films appear milky white due to multiple scattering phenomena from dispersed droplets. The initial starting mixture in the one-phase region appears clear due to absence of phase separation. Thus, a loss in clarity, as noted by visual examination, can be construed as evidence of phase separation. This rough optical method was used to corroborate results obtained by FTIR imaging. Starting with a 50 wt % LC sample, samples of progressively decreasing LC concentration were prepared and cured at different temperatures. The concentration of LC lies between definitely phase-separated and wholly clear samples for different temperatures in Figure 11. It is difficult to judge whether phase separation has occurred in certain samples and hence the values plotted have a large spread as given by the error bars. Comparing results from the imaging data and by visual examination, it can be seen that the spectrometer data agree with the optical method. Spectroscopically determined solubility levels were larger. This may be due to the poorer resolution of the spectrometer. Indeed, the solubility levels for larger droplet sizes are closer to optically determined ones.

It is well-documented that the electrooptic properties of PDLC systems depend strongly on the size and shape of the droplets.[42,43] In classical PIPS methods, it is also observed that concentration of liquid crystal in the initial mixture, temperature of polymerization, and cure rate determine droplet size.[16,44] In the proposed method droplet size is manifested as a kinetic factor that can be controlled by varying a process parameter, i.e., time of cooling. It is also important to note that control over droplet size is independent of the rate of polymerization. This is in marked contrast with current PIPS methods where the development of smaller droplet sizes is induced by rapid polymerization of the matrix or by polymerization at higher temperatures. Larger droplets are obtained either by using a larger liquid crystal fraction or by slower polymerization rates. Both approaches affect matrix solubility. The method outlined in this paper allows tailoring of droplet size without any change in composition of the two phases. Moreover, time is the easiest process parameter to change as opposed to UV intensity or curing temperature. Thus, the method affords even greater flexibility and ease of formation.

As polymerization proceeds, the quench depth continuously increases as the binary phase diagram rises to higher temperatures. This may be expected to lead to multiple phase separation and a continuously varying domain composition. Phase separation will start at the point of time when the polymerization temperature lies on the coexistence curve and slow to a negligible rate close to gelation. This is evidenced by the varied and nonuniform droplet size distributions seen in some studies for an UV curable system.[24] A large polydispersity in sizes is also seen in our systems for large cooling times, probably a result of coalescence and well as factors outlined above. Smaller cooling times at the lower temperature showed a narrow droplet size distribution. LC phase separated by curing was, thus, probably not a very sizable fraction. Clearly, polymerization at lower temperatures would favor less phase separation due to polymerization. Another strategy to control droplet size may be to control coalescence. Starting with an initial mixture that contains a smaller weight fraction of the liquid crystal, coalescence may be reduced. Coalescence may also be prevented by the use of surface-active agents as used for thermoplastics. However, this would increase LC solubility in the matrix and be counterproductive. Thus, it appears that narrow size distribution may be obtained by lowering temperature and limiting prepolymerization standing time.

Of greater concern than the development of a broad size distribution is secondary phase separation induced in already phase-separated domains. As explained above, the coexistence curve shifts upward on polymerization. Thus, the already phase-separated domains may undergo another decomposition; small inclusions may appear inside the original liquid crystal domains, and small LC-rich droplets may appear in the matrix. This situation is similar to that of a two-step temperature quench for thermoplastics[45] and has been observed for a polymer liquid crystal system with a thermoplastic matrix[46] as well as a polymerizing thermosetting matrix.[47] Polymer chains are supposedly excluded totally from the dispersed phase.[48] This should be true for a highly cross-linkable thermoset like NOA65. However, oligomer dissolved in the liquid crystal may also polymerize, increase its molecular weight, and, hence, diffuse out of LC domains at a much slower rate. This may especially be true while the system is first phase separated and then polymerized. To determine whether our process did result in such structures, we also examined large LC domains obtained by long time cooling at a larger quench. No evidence of a secondary phase separation was found as the regions within the droplets were homogeneous and, on an average, spectroscopically identical to other droplets' interior regions. Any residual islands of matrix-rich regions, if they indeed formed, probably migrated to the boundary before images were acquired. This phenomenon has also been reported.[46] However, in some mid-sized droplets, islands of NOA65 were observed. This could possibly be the result of their being polymerized and/or anchored to the boundary layer. Some irregularity is seen at the boundary of larger droplets which could be due to diffused NOA65 collecting at the boundary.

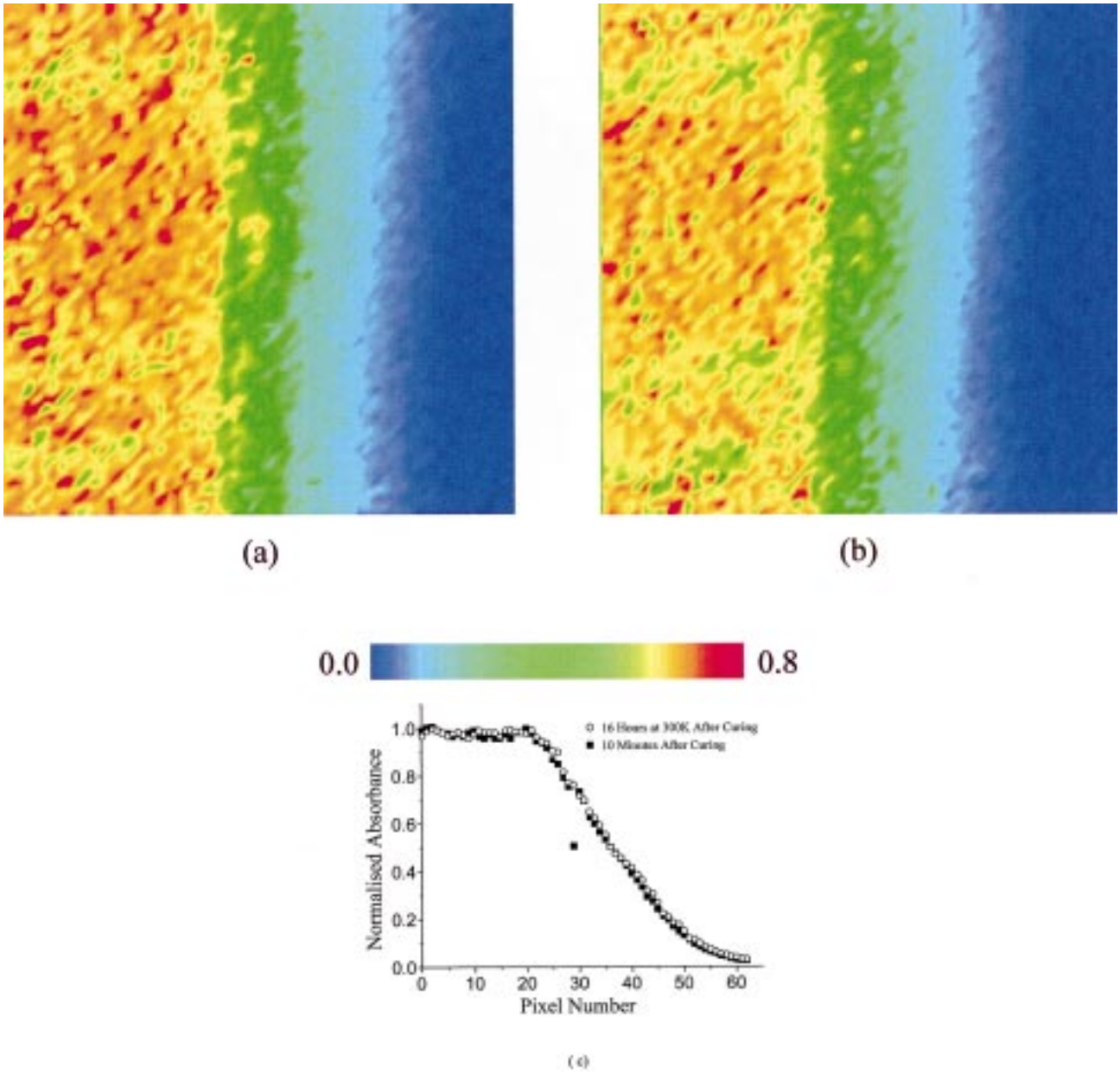

Figure 12. Infrared images of NOA65 cured at 255 K after allowing liquid crytsal to diffuse into it for 2.5 h: (a) obtained 10 min after curing was stopped, (b) obtained after being kept at 300 K for 16 h, and (c) concentration profile for the nitrile band.

We did not observe any change in position of such domains with time due to Brownian motion. The conversion of the thiol group for dissolved polymer chains could not be determined in these sets of experiments due to their low concentration inside the droplets. The NOA65-rich islands in the droplets were no more than 10 μm across (one pixel) and were seen almost exclusively in samples polymerized at 270 K. This is probably due to the higher NOA65 concentration in the droplets at 270 K as opposed to lower levels obtained at 255 K. Given the low NOA65 concentration, polymer walls will not likely form inside droplets. A few walls were seen in some droplets, but these were probably due to coalescence being arrested by gelation. Secondary phase separation does not appear to be important for droplet homogeneity for low enough temperatures. Similarly, small LC-rich droplets may appear in the matrix, and this would induce a more bimodal type of distribution. We did not notice any large-scale appearance of such droplets of size greater than approximately 2 μm (limit of our optical microscope resolution) but did observe a small number of such droplets. Their composition may be expected to be the same as that of the other droplets. They, too, were observed mainly in the 270 K samples. These and other morphological aspects are considered in our next publication on the two-phase method.[40]

The final chemical aspect to be considered in this method is whether the formed structures are stable and whether, with time, solubility would revert to a structure determined by temperature of use. Confirmatory sets of experiments were carried out to determine gelation-imparted stability of dispersed domains. Given the typical domain size and its corresponding diffusive boundary interphase of a PDLC, changes in the boundary layer would have to be drastic for observation. To maximize potential for mobility and observation of changes, a one-dimensional diffusion profile was examined.[8] This simulates an essentially infinite PDLC droplet with a large boundary layer. After allowing E7 to diffuse into unpolymerized NOA65 at 255 K for

approximately 150 min, the sample was subjected to UV radiation in the same manner as experiments on PDLCs at that temperature. After carefully drying the surface to get rid of condensed moisture, the region of contact was imaged. This sample was left undisturbed for 16 h and imaged again. As can be seen by comparing both images obtained by plotting the nitrile band (Figure 12a,b), there appears to be little physical change in the boundary layer. Examining average concentration profiles extracted from the images (Figure 12c), the interphase has very nearly the same concentration profile for both cases. The normalizing absorbance is 0.8 au for both cases.

The electrooptic properties, morphology, and chemical composition of each phase are determined by relative time scales of polymerization and phase separation which affect LC domain and molecular mobility. However, there are four different time scales of importance in the formation of PDLCs by PIPS: the time required for the mixture to achieve thermal equilibrium before phase separation (equilibration time), the rest time after mixing of components and before onset of cure (prepolymerization time), the time of cure up to gel point (polymerization time), and the time scale for phase separation due to polymerization. Each of these time scales is influenced by the temperature profile the mixture is subjected to. For miscible monomers, the prepolymerization time is unimportant, and there are only two time scales. Clearly, the equilibration time must be as small as possible. We conducted different sets of experiments with coverslips as PDLC film substrates and salt plates as substrates. In both experiments solubility was found to be the same. Equilibration time can be safely assumed similar for these substrates. The time scale of prepolymerization rest is, almost exclusively, expected to determine droplet size for the two-phase method. The smaller this time scale is, the faster is the growth of droplets. Ideally, the rest time must be large enough to be several orders of magnitude larger than the equilibration time but must be small enough to allow the rest time to be used as a viable process variable for droplet size control. The polymerization time must again be as small as possible to allow quick processing and fast freezing of structures formed. The time scale for phase separation due to polymerization must again be much larger than polymerization time. This would prevent formation of secondary structures and result in a uniform droplet size distribution. Thus, transition process properties are somewhat different for this method as opposed to those required for the conventional PIPS method.

In this paper, we have focused on an UCST system. To the best of our knowledge, there is no PDLC forming system that has a LCST type of phase diagram. This type of diagram is usually found only in high polymer mixtures. In those thermosetting systems, the LCST coexistence curve shifts to lower temperatures with conversion.[49] In such a case, our method would call for raising the temperature to the two-phase region and polymerization at elevated temperatures as opposed to depressed temperatures used in the paper. Thus, the outlined methodology is highly flexible and can be applied to any system where lower miscibility of phase-separated domains is desirable.

Conclusions

In this paper, we demonstrate the importance of temperature regimes on the photoinduced polymerization process of PDLC formation. A new route to produce PDLCs with reduced matrix LC solubilities by polymerizing in the two-phase region is suggested. This method has been demonstrated to successfully reduce matrix solubility of the liquid crystal. PDLCs analyzed for morphological structures showed domain sizes to be fairly controlled and uniform over the film. Large "puddles" or anomalously large droplets were not seen for cooling times of about 12 h. The LC domain size is related to the standing time of the mixture before polymerization. Qualitatively, the longer the standing time, the larger was the domain size. Polydispersity in sizes was not very great for smaller cooling times. Thus, the resultant morphology may not always be "undesirable" for polymerization in the two-phase regime. This two-phase polymerization technique has the added flexibility of potentially controlling droplet size by simply adjusting the time of cooling. Dispersions across a dimensional spectrum of 2 orders of magnitude can be obtained by appropriate cooling times. Additionally, the phase composition for all domain sizes obtained is the same. Thus, the process has allowed decoupling of the polymerization process (which determines thermodynamic limits of solubility) from the process of phase separation (which determines kinetically achievable solubility and domain size). This process lays out a very attractive route to produce samples for studies that examine droplet size effects on PDLC properties without the complicating effects introduced by phase composition changes. A new technique, FTIR imaging, has been demonstrated to be a powerful tool for characterizing complex polymer dispersions and for monitoring phase composition in a multiphase system. In conjunction with task specific data processing and calibration, the technique has proven to be a very successful one for nondestructive, noninvasive spatially resolved chemical species detection and quantification.

Acknowledgment. Funding for the project was provided by the National Science Foundation Center for Advanced Liquid Crystalline Optical Materials (ALCOM) Grant Number NSF DMR89-20147. We thank Claire Kovacs for carrying out experiments to determine the phase separation curve for a curing NOA65-E7 mixture by optical examination.

References and Notes

(1) *Liquid Crystals-Applications and Uses*; Bahadur, B., Ed.; World Scientific Publishing: Singapore, 1990; Vol. 1.
(2) Doane J. W.; Golemme, A.; West, J. L.; Whitehead, J. B.; Wu, B. G. *Mol. Cryst. Liq. Cryst.* **1988**, *165*, 511.
(3) Golovataya, N. M.; Kurik, M. V.; Lavrentovich, O. D. *Liq. Cryst.* **1990**, *7*, 287.
(4) Challa, S. R.; Wang, S.-Q.; Koenig, J. L. *J. Therm. Anal.* **1995**, *45*, 1297.
(5) Snively, C. M.; Koenig, J. L.; Chen; Palmer, R. A. *Mol. Cryst. Liq. Cryst.* **1996**, *289*, 11.
(6) Bosc, D.; Trubert, C.; Vinouze, B.; Guilbert, M. *Appl. Phys. Lett.* **1996**, *68*, 2489.
(7) Ahn, W.; Kim, C. Y.; Kim, H.; Kim, S. C. *Macromolecules* **1992**, *25*, 5002.
(8) Challa, S. R.; Wang, S.-Q.; Koenig, J. L. *Appl. Spectrosc.* **1996**, *50*, 1339. Challa, S. R.; Wang, S.-Q.; Koenig, J. L. *Appl. Spectrosc.* **1997**, *51*, 10.
(9) Vaz, N. A.; Smith, G. W.; Montgomery, G. P., Jr. *Mol. Cryst. Liq. Cryst.* **1987**, *146*, 17.
(10) Vaz, N. A.; Montgomery, G. P., Jr. *J. Appl. Phys.* **1987**, *62*, 3161.
(11) Rout, D. K.; Jain, S. K. *Jpn. J. Appl. Phys.* **1991**, *30*, L 1412.
(12) Carpaneto, L.; Ristango, A.; Stagnaro, P.; Valenti, B. *Mol. Cryst. Liq. Cryst.* **1996**, *290*, 213.
(13) Matsuyama, A.; Kato, T. *J. Chem. Phys.* **1998**, *108*, 2067.

(14) Chan, P. K.; Rey, A. D. *Macromolecules* **1996**, *29*, 8934.
(15) Lin, B.; Taylor, P. L. *Polymer* **1996**, *37*, 5099.
(16) West, J. L.; Golemme, A.; Doane, J. W. U.S. Patent 4673255.
(17) Vaz, N. A.; Smith, G. W. *Mol. Cryst. Liq. Cryst*. 243.
(18) Smith, G. W. *Mol. Cryst. Liq. Cryst*. **1993**, *225*, 113.
(19) Boots, H. M. J.; Kloosterboer, J. G.; Serbutoviez, C.; Touwslager, F. J. *Macromolecules* **1996**, *29*, 7683. Serbutoviez, C.; Kloosterboer, J. G.; Boots, H. M. J.; Touwslager, F. J. *Macromolecules* **1996**, *29*, 7690.
(20) West, J. L. *Mol. Cryst. Liq. Cryst*. **1988**, *157*, 427.
(21) Doane, J. W.; Vaz, N. A.; Wu, B. G.; Zumer, S. *Appl. Phys. Lett*. **1986**, *48*, 269.
(22) Coates, D.; Greenfield, S.; Sage, I. C.; Smith, G. In *Liquid Crystal Display and Applications*; SPIE: Bellingham, WA, 1990; Vol. 1257, p 37.
(23) Smith, G. W. *Int. J. Mod. Phys. B* **1993**, *7*, 4187.
(24) Smith, G. W. *Phy. Rev. Lett*. **1993**, *70*, 198.
(25) Lovinger, A. J.; Amundson, K. R.; Davis, D. D. *Chem. Mater*. **1994**, *6*, 1726.
(26) Challa, S. R.; Wang, S.-Q.; Koenig, J. L. *Appl. Spectrosc*. **1995**, *49*, 267.
(27) McFarland, C. A.; Koenig, J. L.; West, J. L. *Appl. Spectrosc*. **1993**, *47*, 321.
(28) Treado, P. J.; Levin, I. W.; Lewis, E. N. *Appl. Spectrosc*. **1992**, *46*, 553.
(29) Bhargava, R.; Wang, S.-Q.; Koenig, J. L. *Appl. Spectrosc*. **1998**, *52*, 323.
(30) Bio-Rad, Digilab Laboratories, Cambridge, MA.
(31) RSI Inc., 2995 Wilderness Place, Boulder, CO 80301.
(32) BDH Chemical Company, Poole distributed by EM Industries, Hawthorne, NY 10532.
(33) Norland Products Inc., P.O. Box 145, North Brunswick, NJ 08902.
(34) Smith, G. W. *Mol. Cryst. Liq. Cryst*. **1991**, *196*, 89.
(35) Chiou B.-S.; Khan, S. A. *Macromolecules* **1997**, *30*, 7322. Chiou, B.-S.; English, R. J.; Khan, S. A. *Macromolecules* **1996**, *29*, 5368.
(36) Kim, J. Y.; Palffy-Muhoray, P. *Mol. Cryst. Liq. Cryst*. **1991**, *203*, 93.
(37) Smith, G. W. *Mol. Cryst. Liq. Cryst*. **1991**, *196*, 89.
(38) Montgomery, G. P.; Vaz, N. A.; Smith, G. W. *Mol. Cryst. Liq. Cryst*. **1993**, *225*, 131.
(39) Tanaka, H. *J. Chem. Phys*. **1996**, *195*, 10099.
(40) Bhargava, R.; Wang, S.-Q.; Koenig J. L. Manuscript under preparation.
(41) Smith, G. W. *Mol. Cryst. Liq. Cryst*. **1994**, *239*, 63.
(42) Vaz, N. A.; Smith, G. W.; Montgomery, G. P. *Mol. Cryst. Liq. Cryst*. **1987**, *146*, 17.
(43) Vaz, N. A.; Smith, G. W.; Montgomery, G. P. *Mol. Cryst. Liq. Cryst*. **1987**, *146*, 1.
(44) Vaz, N. A.; Smith, G. W. *Liq. Cryst*. **1988**, *3*, 543.
(45) Okada, M.; Kwak, K. D.; Nose, T. *Polym. J*. **1992**, *24*, 215.
(46) Casagrande, C.; Fabre, P.; Guedeau, M. A.; Veyssie, M. *Europhys. Lett*. **1987**, *3*, 73.
(47) Kim, J. Y.; Cho, C. H.; Palffy-Muhoray, P.; Mustafa, M.; Kyu, T. *Phys. Rev. Lett.* **1993**, *71*, 2232.
(48) Shen, C.; Kyu, T. *J. Chem. Phys*. **1995,** *102*, 556.
(49) Williams, R. J. J.; Rozenberg, B. A.; Pascault, J.-P. *Adv. Polym. Sci*. **1997**, *128*, 95.

MA981542S